Journal of Superconductivity and Novel Magnetism
https://doi.org/10.1007/s10948-018-4974-3

ORIGINAL PAPER

Spin Glass Behavior in $La_{0.7}Ca_{0.23}Sr_{0.07}MnO_3$ Nanofibers Obtained by Electrospinning

L. A. Burrola-Gándara[1] · L. Vázquez-Zubiate[1] · D. M. Carrillo-Flores[1] · J. T. Elizalde-Galindo[1]

Received: 2 November 2018 / Accepted: 12 December 2018

Abstract
This work contributes to the development of new nanostructured mixed valence manganites and to explore and optimize their magnetic properties at 1-D level. Nanofibers of $La_{0.7}Ca_{0.23}Sr_{0.07}MnO_3$ manganite were fabricated using the electrospinning method and three different heat treatments to determine how the nanostructure affects its thermomagnetic behavior. From scanning electron microscopy, nanofibers morphology was observed and average diameters of 75, 94, and 97 nm were identified after heat treatments of 973, 1073, and 1173 K, respectively. According to X-ray diffraction technique, a single-phase orthorhombic structure was defined for each sample. Average crystallite sizes were determined as 47, 49, and 58 nm. A ferromagnetic to paramagnetic transition with Curie temperatures of 297, 305, and 314 K were identified, respectively. Furthermore, a glassy state was induced by nanofibers agglomeration. The spin glass and irreversible temperatures diminished as the magnetic field was increased and a highly anisotropic state was evidenced for all samples. Thermomagnetic behavior in manganites showed to be significantly influenced by the one-dimensional structure and exposed how the dimensionality proportionated by the fabrication method can be used to adjust magnetic properties.

Keywords Manganite · Nanofibers · Spin glass · Thermomagnetic behavior

1 Introduction

For a long time, perovskite manganites have been investigated for their physical properties. In this group, mixed valence manganites with general formula $R_{1-x}A_xMnO_3$ (where R is a rare-earth metal, and A is an alkaline-earth metal) have phase diagrams where paramagnetic (PM), ferromagnetic (FM), and antiferromagnetic (AFM) phases, appear together with complex ones like spin-glass [1]. The magnetic properties of mixed valence manganites are strongly dependent on the coupling between Mn^{3+} and Mn^{4+} ions, specifically of Mn–O bond distance and Mn–O–Mn bond angle [2,3]. In these materials, the double-exchange interaction (DEI) helps to explain the appearance of ferromagnetic ordering occurred when electrons are transported from Mn^{3+} ions to Mn^{4+} ions through oxygen atoms [3]. Furthermore, the strong relationship between structural, magnetic, and electric degrees of freedom presented by these complex oxides are relevant for technological applications. Recently, research on magnetic nanostructures has increased due to their original physical properties, which compared with the bulk form are significantly different [4, 5]. Also, their potential application in areas such as photonics, microelectronics, magnetic, and spintronic devices has attracted even more research interest in one-dimensional manganite nanostructures like nanorods, nanofibers, nanowires, and nanotubes [6–8]. Consequently, adjust, optimize, and control the nanostructure, morphology, and size of these materials are essential for their potential technological applications [4]. To synthesize nanofibers, several fabrication methods like template synthesis, self-assembly, phase separation, and electrospinning have been employed [6]. The research interest in electrospinning of ceramics has increased

✉ L. A. Burrola-Gándara
andres.burrola@gmail.com

L. Vázquez-Zubiate
lizethvazquezzubiate@gmail.com

D. M. Carrillo-Flores
diana.carrillo@uacj.mx

J. T. Elizalde-Galindo
jose.elizalde@uacj.mx

[1] Instituto de Ingeniería y Tecnología, Universidad Autónoma de Ciudad Juárez, Av. Del Charro 450 norte, 32310 Ciudad Juárez, Chihuahua, México

Published online: 02 January 2019

because of its simplicity and useful way to synthesize the 1-D nanostructure and the low fabrication cost [4, 6]. Furthermore, adjusting the electrospinning parameters such as the precursor concentration, the solution viscosity, the needle gauge, the solution flow rate, the applied potential, and the distance of the applied potential can be used to control the fiber sizes [9]. In this work, nanofibers of $La_{0.7}Ca_{0.23}Sr_{0.07}MnO_3$ manganite were successfully fabricated using the electrospinning method, with the purpose of identifying how the nanostructure obtained and the heat treatment applied, influence their thermomagnetic properties.

2 Materials and Methods

To obtain $La_{0.7}Ca_{0.23}Sr_{0.07}MnO_3$ nanofibers, a precursor solution was made starting from stoichiometrically weighed La, Ca, Sr, and Mn acetates dissolved in water at 0.1 M concentration. Subsequently, 20% of polyvinylpyrrolidone (PVP) polymer was added to the solution and mixed to attain an appropriate viscosity. A syringe connected to a hose with an end in a 22-gauge needle was used to transport the solution. Using a fluid flow of 0.1 ml/h, assigned with a pump, a drop of the solution was set in the tip of the needle. Then, from a vertical distance of 15 cm between the 22-gauge needle, made of stainless steel, and an aluminum deposit plate, the electric field of 15 kV was set to extrude the fibers. After that, the fibers were collected and process by the corresponding heat treatments. The heat treatments were applied using a heating ramp of 1 K/min, followed for an isotherm of 973, 1073, and 1173 K applied for 1.5 h. Nanofibers were obtained utilizing a Tong Li Tech Co. electrospinning equipment model TL-Pro. The phase formation and crystal structure of the nanofibers were verified by X-ray diffraction (XRD) technique, using a Panalytical diffractometer model X'Pert Pro-MPD. Whereas, nanofibers diameters and morphology were identified by scanning electron microscopy (SEM), through a JEOL 6010 LV microscope. Zero-field cooling and field cooling thermomagnetic curves at magnetic fields of 2, 5, 10, and 15 mT and M vs. H measurements were carried out in a Quantum Design Versalab, with a vibrating sample magnetometer probe.

3 Results and Discussion

X-ray diffraction patterns for $La_{0.7}Ca_{0.23}Sr_{0.07}MnO_3$ nanofibers heat-treated at 973, 1073, and 1173 K respectively are exposed in Fig. 1. According to these, a single-phase orthorhombic structure was identified with PDF 01-071-5292 file for each sample. The peaks, more defined and their narrowing as heat treatment is increased, were evidence of crystallization and growth. Using the Scherrer equation ($d = k\lambda/\beta \cos\theta$), the crystallite sizes were estimated as 47, 49, and 58 nm for 973, 1073, and 1173 K heat-treated samples respectively. The time

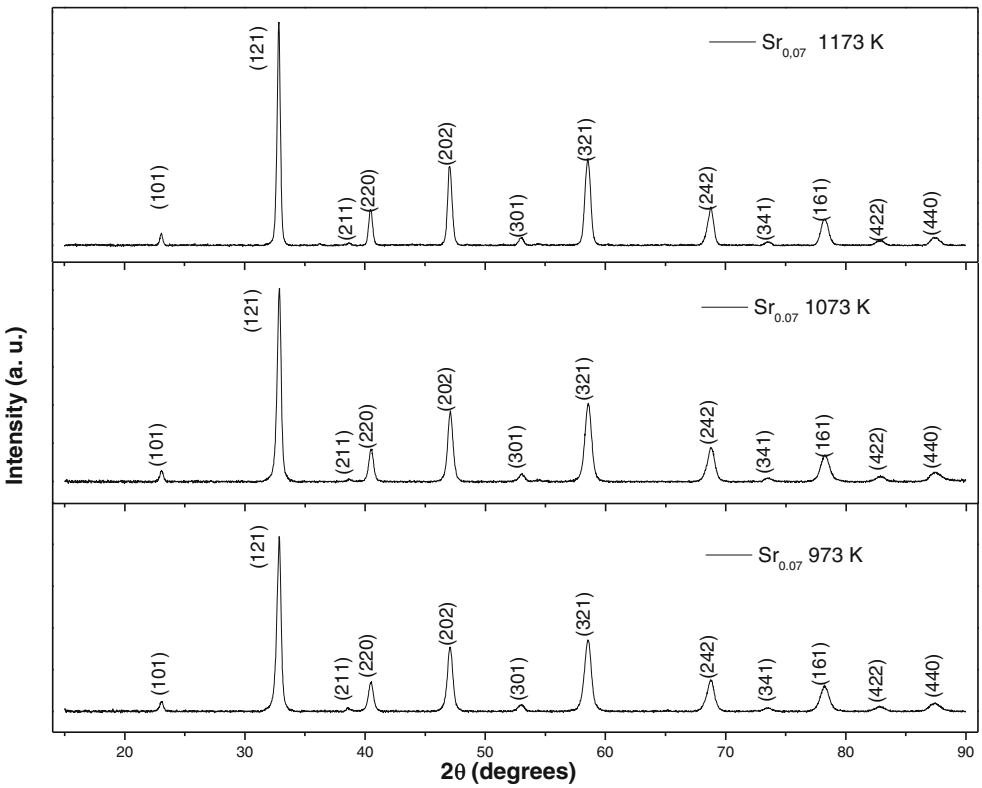

Fig. 1 X-ray diffraction patterns for $La_{0.7}Ca_{0.23}Sr_{0.07}MnO_3$ nanofibers heat treated at 973, 1073, and 1173 K

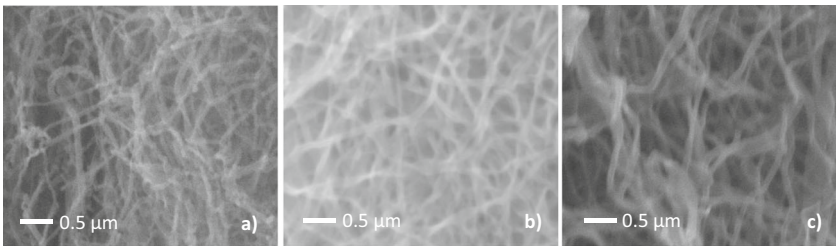

Fig. 2 Micrographs obtained from secondary electrons in SEM microscopy for $Sr_{0.07}$ samples heat-treated at (a) 973 K, (b) 1073 K, (c) 1173 K with × 30000 of magnification

to reach the isotherm increases for each sample as heat treatment temperature rises. Therefore, the heating ramp of 1 K/min extends the heat exposure and increases the crystal growth. The strain represented by the slope in Williamson-Hall equation $\beta_{hkl}Cos\theta_{hkl} = k\lambda/D_{W-H} + 4\varepsilon sin\theta_{hkl}$, [10] for the nanofibers of $La_{0.7}Ca_{0.23}Sr_{0.07}MnO_3$ heat treated at 973, 1073, and 1173 K demonstrates that there are no strain present. Thus, any effect due strain can be considered.

Micrographs acquired for $La_{0.7}Ca_{0.23}Sr_{0.07}MnO_3$ nanofibers at (a) 973 K, (b) 1073 K, and (c) 1173 K heat treatments respectively are shown in Fig. 2. The micrographs show agglomerates of nanofibers, related with the extrusion on the aluminum deposit plate with different diameter distribution according to the heat treatment. The average fiber diameter, measured from these micrographs, was 75, 94, and 97 nm for 973, 1073, and 1173 K heat-treated samples respectively. The diameter growth demonstrates that PVP polymer is already calcined, by the time the isotherm temperature was reached in all samples, which also supports the crystal growth.

The temperature dependence of magnetization was measured for $La_{0.7}Ca_{0.23}Sr_{0.07}MnO_3$ nanofibers, with heat treatments of 973, 1073, and 1173 K, using zero-field cooling

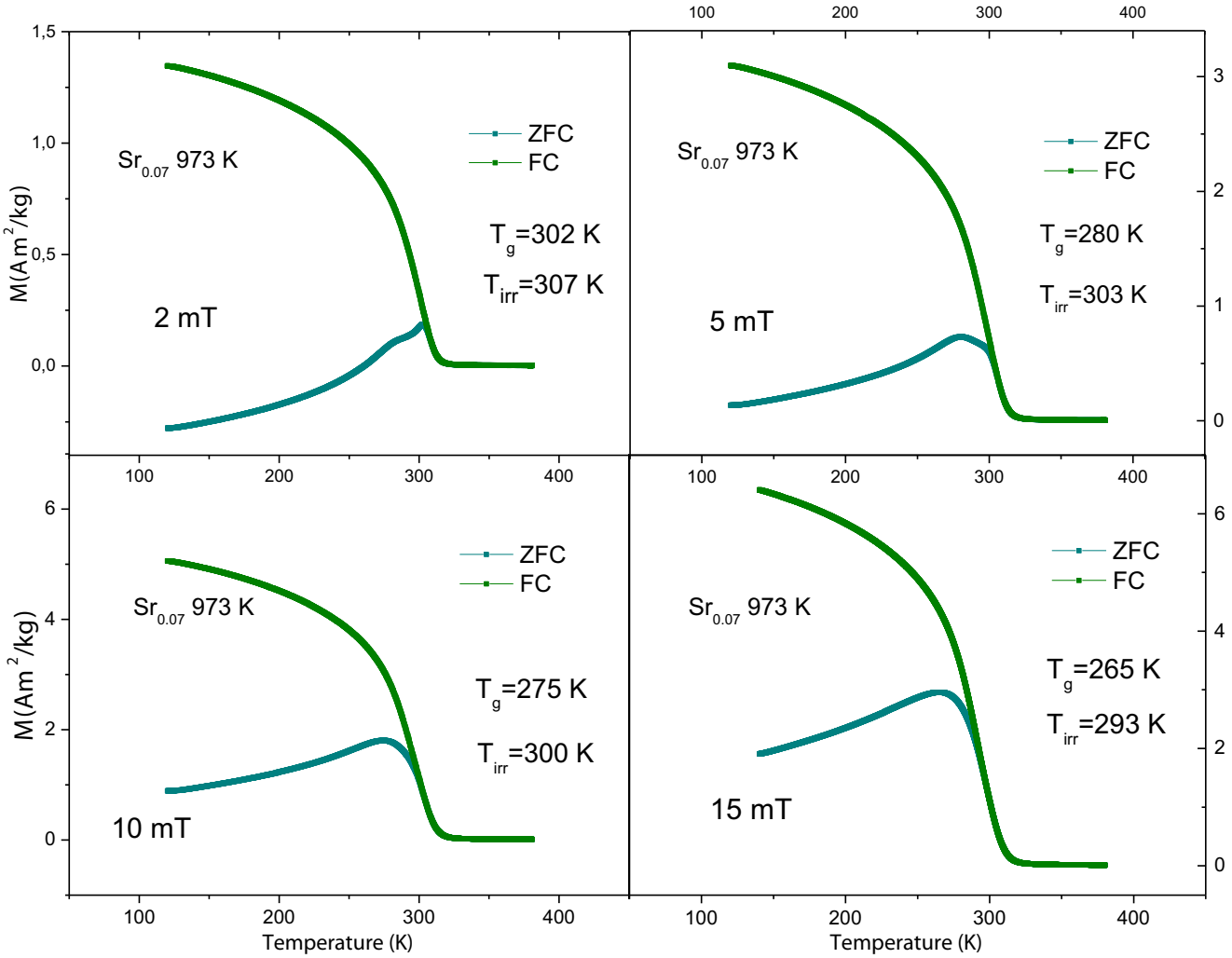

Fig. 3 ZFC and FC curves for $Sr_{0.07}$ sample heat treated at 973 K, with applied magnetic fields of 2, 5, 10, and 15 mT

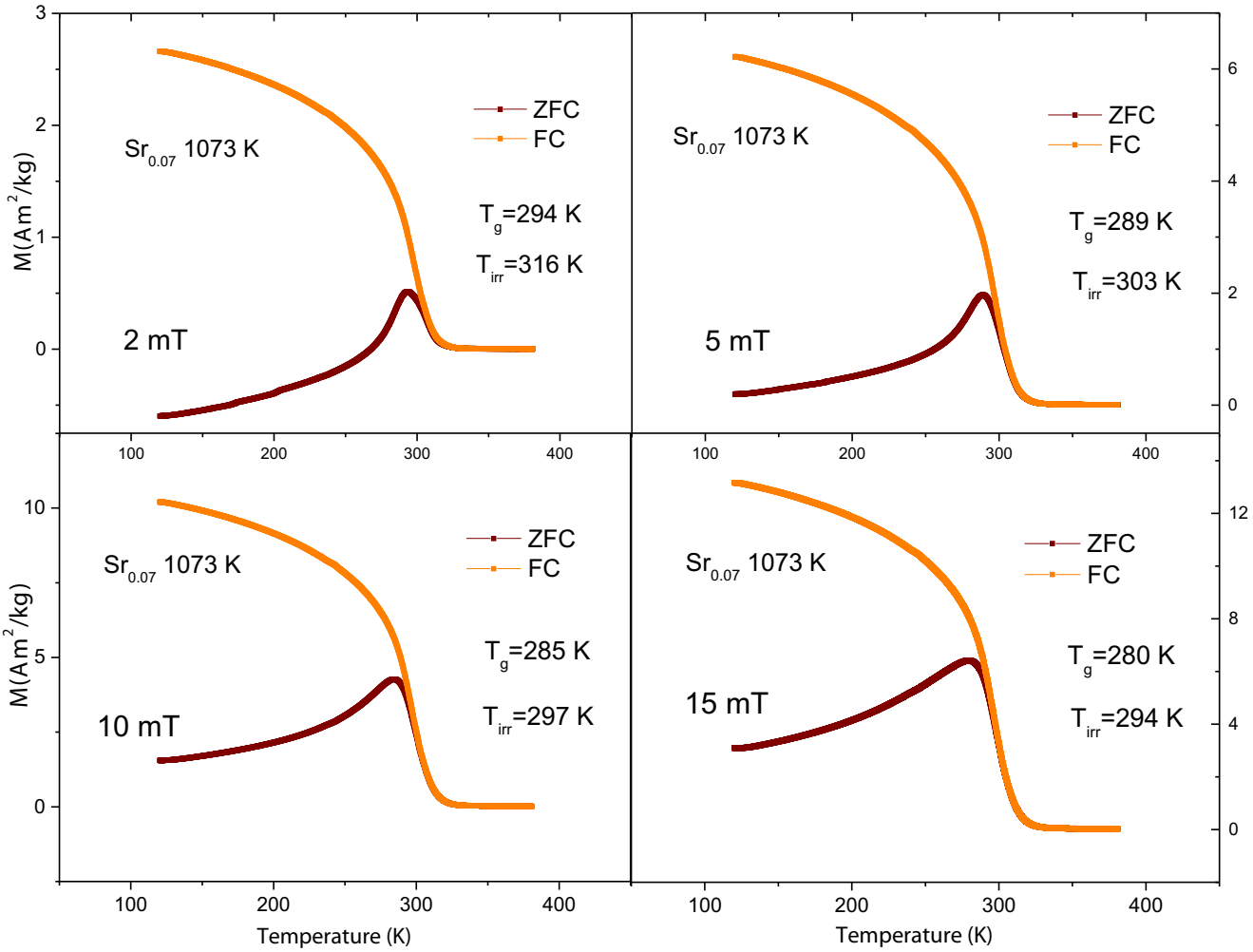

Fig. 4 ZFC and FC curves for $Sr_{0.07}$ sample heat treated at 1073 K, with applied magnetic fields of 2, 5, 10, and 15 mT

(ZFC) and field cooling (FC) processes. These ZFC-FC magnetization curves were measured for magnetic fields applied of $\mu_0 H$= 2, 5, 10, and 15 mT in a temperature range from 110 to 380 K, and are exposed in Figs. 3, 4, and 5 respectively.

Figure 3 illustrates ZFC-FC curves for $Sr_{0.07}$ nanofibers heat treated at 973 K. All graphs for this sample display a ferromagnetic to paramagnetic transition, where a Curie temperature (T_C) of ~ 297 K remains independently of the magnetic field applied. A bifurcation between ZFC and FC curves that diverges for lower temperatures can be observed for every magnetic field applied. The divergence of ZFC-FC curves for low temperatures has been found in disordered systems like spin glasses or superparamagnetic nanoparticles [11, 12]. For this sample, the separation between curves starts at irreversibility temperature (T_{irr}) and diverges strongly for lower temperatures in each magnetic field applied. Such strong divergence occurred among ZFC-FC curves in this sample is considered a typical behavior of spin-glasses systems [13, 14]. Furthermore, there is a broad cusp in ZFC curves displayed for lower temperatures in each magnetic field applied, which is also considered a characteristic behavior of disordered systems [14–16]. This cusp has place on the called spin-glass freezing temperature (T_g), below which the system enters to glassy state. The cusp widens as magnetic field increases and T_g shifts to lower temperatures when the magnetic field rises. Typically, in standard spin-glasses systems, T_{irr} is very close to T_g, but for this $La_{0.7}Ca_{0.23}Sr_{0.07}MnO_3$ nanofibers system, T_g and T_{irr} remain apart from each other for magnetic fields applied, indicating the appearance of a cluster glass state for low temperatures as pointed out by several authors [11, 13, 14]. The T_g located in ZFC curves diminishes from 302 to 265 K, as the magnetic field increases and is related with the decrease of crystal-field anisotropy. According to this, when magnetic field increases, the energy barrier due to magnetic anisotropy diminishes, and then a smaller amount of thermal energy is required to overcome the

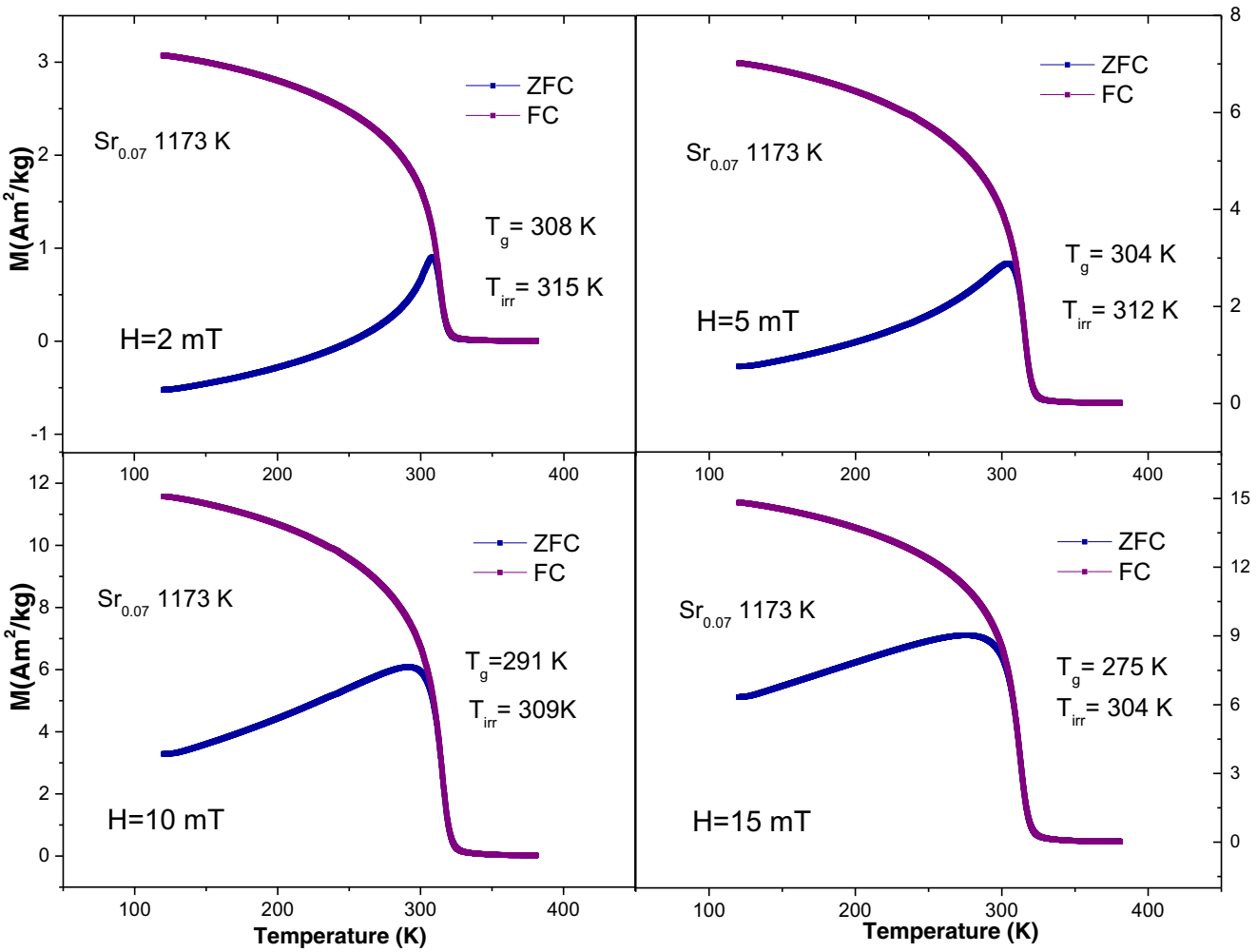

Fig. 5 ZFC and FC curves for $Sr_{0.07}$ nanofibers heat treated at 1173 K with applied magnetic fields of 2, 5, 10, and 15 mT

energy barrier, which causes a decreasing in T_g temperature [17]. The small magnetization response visualized in ZFC curves for low temperatures demonstrates that the applied magnetic fields are not strong enough to rotate the spins easily on the magnetic field direction, which is related with a high anisotropic system [18].

ZFC-FC curves are shown in Fig. 4 for $Sr_{0.07}$ nanofibers heat treated at 1073 K. A FM to PM transition is depicted with a constant Curie temperature of ~305 K for 2, 5, 10, and 15 mT magnetic fields applied respectively. A strong divergence between ZFC and FC curves is evidenced for this sample, which represents an irreversibility behavior [19] where T_{irr} temperatures diminish as applied magnetic fields increase. The cusp in ZFC curve and the characteristic strong separation between ZFC and FC curves, related to cluster-glass behavior [20], remains in $Sr_{0.07}$ sample heat treated at 1073 K for every magnetic field applied. From ZFC processes, a random magnetization of the sample occurs around $T_C = 305$ K and remains upon cooling to 110 K because spins lack enough thermal energy to rotate, and when the temperature increases, thermal energy unlocks the spins aligning them in the direction of the applied field increasing magnetization. This unlocking process starts first with small particles and later with bigger particles [21]. Therefore, comparing T_g peaks between 1073 K and 973 K heat-treated samples. The narrower T_g peaks, for all magnetic fields applied in the 1073 K heat-treated sample, are related with a more homogeneous particle size distribution inside the nanofibers, since small particles were reduced. Magnetic anisotropy remains high for nanofibers heat treated at 1073 K as can be seen in FC curves, where magnetization increases as temperature diminish [18].

ZFC-FC curves are observed in Fig. 5 for $Sr_{0.07}$ nanofibers heat treated at 1173 K. The sharp increase in magnetization around T_C ~314 K remains for each magnetic field applied, indicating a PM to FM transition. Also, in comparison with 973 and 1073 K heat-treated samples, a steep slope at T_C can be noticed, representing a higher defined PM to FM transition. This steep slope at T_C is related with a more homogeneous

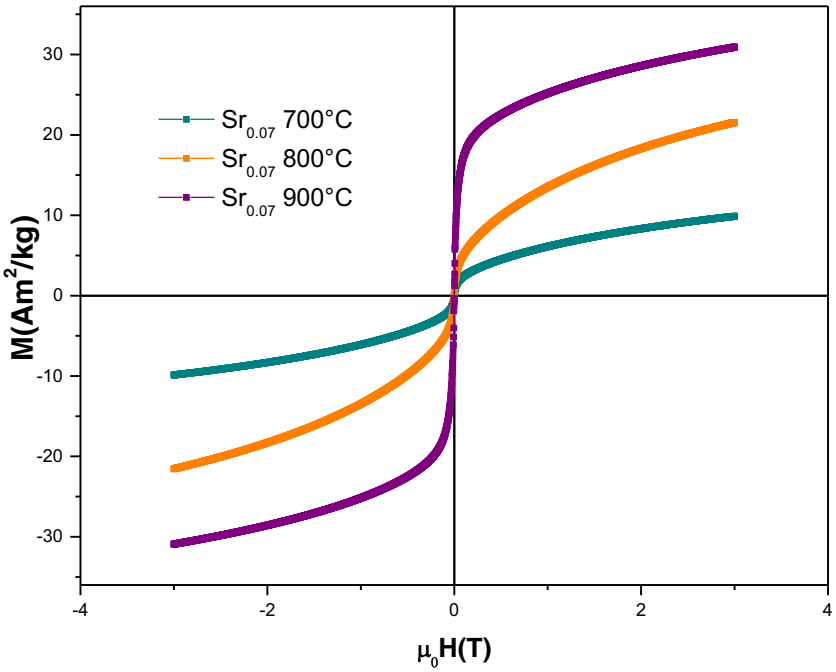

Fig. 6 M vs $\mu_0 H$ curves for $Sr_{0.07}$ samples heat treated at 973, 1073, and 1173 K under an applied magnetic field from 1 to 3 T measured at 300 K

particle size distribution inside the nanofibers of the sample. Moreover, T_C value is the higher among the samples, which is attributed to the strengthening of double-exchange interaction via crystallite growth, since this interaction depends on Mn–O bond distance and Mn–O–Mn bond angle. The strong divergence of ZFC-FC curves at low temperatures and the cusp displayed in ZFC curves for each magnetic field applied, still appear in this sample, supporting its glassy nature [22]. Also, T_g and T_{irr} temperatures remain separated for each applied magnetic field, evidencing cluster-glass behavior. This feature is supported by the rapid rise in magnetization in FC curves, which could be associated with the occurrence of a short-range FM ordering, forming FM clusters [12]. Observing closely, T_{irr} and T_g tend to separate from each other when magnetic field increases, which was attributed to a more uniform reduction of crystal-field anisotropy, since for this sample, a more homogeneous particle size distribution is present.

High magnetic anisotropy is a representative feature of spin-glass systems. In ZFC and FC processes for this system, such high magnetic anisotropy is represented by the strong divergence between these curves [23]. In FC process, when the sample is cooled in the presence of a magnetic field. The random-oriented spins tend to be aligned in the magnetic field direction when the sample passes through the Curie temperature. As temperature diminishes, particular spins tend to be aligned with the field and freeze. New spins tend to be aligned with the field in collaboration with previous oriented ones. Also magnetic frustration and magnetic anisotropy rises producing a sudden increase in magnetization. Such sudden increase in magnetization is a particular behavior of spin glasses.

A negative magnetization can be observed in ZFC curves measured at 2 mT for 973, 1073, and 1173 K heat-treated samples respectively. This behavior could be related to the freezing of randomly oriented spin glass clusters, which at low temperatures have a long-term frustration. As nanofibers are agglomerated, interactions in the samples also occur between fibers, producing frustration between random competing interactions among Mn^{3+} and Mn^{4+} ions. Then, negative magnetization could be explained due to the short-range interaction between these ions. When temperature diminishes, short-range interaction rises and a long-term frustration appears. This magnetic frustration promotes that the spin clusters cannot be oriented specifically in a preferred direction [24]. When the clusters interact, they cannot be oriented immediately in the field direction due to a greater magnetic anisotropy energy barrier in the sample and only spin-glass clusters oriented in the opposite direction of the field contribute to the magnetization. The behavior of competing interactions between clusters was gradually overcome, as the increase in temperature provides enough thermal energy to the spins glass clusters to rotate in the direction of the magnetic field applied.

Magnetic field dependence of magnetization for $Sr_{0.07}$ nanofibers, heat treated at 973, 1073, and 1173 K is exposed in Fig. 6. The M (H) curves were measured in a magnetic field from 0 to 3 T at room temperature. As can be seen, magnetization increases faster for low fields and improves as heat treatment increases, then the increase was gradual with further increase in the magnetic field, according to the sample. Magnetic hysteresis loop

of manganites usually exhibits a very high rise in M at low fields and a gradual saturation at high fields. The samples studied here did not show any sign of saturation at $\mu_0 H = 3$ T, which is attributed to the glassy nature of the samples [22]. Besides, the S shape with a positive curvature displayed at low fields for this sample is also a feature of spin glasses [25]. The M (H) curves displayed by ferromagnets and superparamagnets describe a different behavior compared with spin glasses. The effect of increasing the measurement temperature for spin glasses promotes the narrowing of the magnetic hysteresis loop [26, 27]. Hence, the narrow loops, observed for these samples, have an explanation in the measurement temperature (300 K), which is high enough to stretch the loops.

4 Conclusions

Single-phase nanofibers of $La_{0.7}Ca_{0.23}Sr_{0.07}MnO_3$ manganite were successfully obtained with the electrospinning method. With the rise in heating time and temperature of the heat treatments, crystallite growth was noticed from the Scherrer equation with values of 47, 49, and 58 nm respectively and from Williamson-Hall equation, a cero strain value was obtained for $Sr_{0.07}$ nanofibers. Using SEM microscopy, agglomerates of nanofibers were observed in all the samples, showing average fiber diameters of 75, 94, and 97 nm for 973, 1073, and 1173 K heat-treated samples respectively. From ZFC-FC magnetic measurements, a FM-PM transition was identified for all samples, where Curie temperatures of 297, 305, and 314 K were determined according to the heat treatment. The rise in T_C is related to the strengthening of double-exchange interaction via crystallite growth, as, in mixed valence manganite systems, this interaction is directly influenced by the Mn–O–Mn bond angle and Mn–O bond distance of Mn^{3+}–O–Mn^{4+} chains. Thermomagnetic measurements for all samples showed a bifurcation between ZFC-FC curves at the irreversible temperature (T_{irr}), which diverge strongly for lower temperatures. This bifurcation, together with the cusp showed at T_g in ZFC curves for low temperatures, demonstrates the glassy nature of the sample. When the magnetic field was increased in ZFC-FC measurements, T_g shifts to lower temperatures with the increase in the magnetic field, which is associated with the decrease of crystal-field anisotropy. Agglomeration of $La_{0.7}Ca_{0.23}Sr_{0.07}MnO_3$ nanofibers induced both high anisotropy and glassy nature behavior displayed.

Acknowledgements This work was supported by Professor Professional Development Program [F-PROMEP-39/Rev-04] SEP, México.

Compliance with Ethical Standards

Conflict of Interest The authors declare that they have no conflict of interest.

References

1. Dang, N.T., Zakhvalinskii, V.S., Kozlenko, D.P., Phan, T.-L., Kichanov, S.E., Trukhanov, S.V., Trukhanov, A.V., Nekrasova, Y.S., Taran, S.V., Ovsyannikov, S.V., Jabarov, S.H., Trukhanova, E.L.: Effect of Fe doping on structure, magnetic and electrical properties $La_{0.7}Ca_{0.3}Mn_{0.5}Fe_{0.5}O_3$ manganite. Ceram. Int. **44**, 14974–14979 (2018). https://doi.org/10.1016/j.ceramint.2018.05.124
2. Ezaami, A., Sellami-Jmal, E., Chaaba, I., Cheikhrouhou-Koubaa, W., Cheikhrouhou, A., Hlil, E.K.: Effect of elaborating method on magnetocaloric properties of $La_{0.7}Ca_{0.2}Ba_{0.1}MnO_3$ manganite. J. Alloys Compd. **685**, 710–719 (2016). https://doi.org/10.1016/j.jallcom.2016.05.332
3. Gómez, A., Chavarriaga, E., Supelano, I., Parra, C.A., Morán, O.: Tuning the magnetocaloric properties of $La_{0.7}Ca_{0.3}MnO_3$ manganites through Ni-doping. Phys. Lett. A. **382**, 911–919 (2018). https://doi.org/10.1016/j.physleta.2018.01.030
4. Zhou, X., Zhao, Y., Cao, X., Xue, Y., Xu, D., Jiang, L., Su, W.: Fabrication of polycrystalline lanthanum manganite ($LaMnO_3$) nanofibers by electrospinning. Mater. Lett. **62**, 470–472 (2008). https://doi.org/10.1016/j.matlet.2007.05.063
5. Hayat, K., Shaheen Shah, S., Yousaf, M., Javid Iqbal, M., Ali, M., Ali, S., Ajmal, M., Iqbal, Y.: Processing, device fabrication and electrical characterization of $LaMnO_3$ nanofibers. Mater. Sci. Semicond. Process. **41**, 364–369 (2016). https://doi.org/10.1016/j.mssp.2015.10.009
6. Hayat, K., Javid Iqbal, M., Rasool, K., Iqbal, Y.: Device fabrication and dc electrical transport properties of barium manganite nanofibers (BMO-NFs). Chem. Phys. Lett. **616-617**, 126–130 (2014). https://doi.org/10.1016/j.cplett.2014.10.046
7. Yensano, R., Pinitsoontorn, S., Amornkitbamrung, V., Maensiri, S.: Fabrication and magnetic properties of electrospun $La_{0.7}Sr_{0.3}MnO_3$ nanostructures. J. Supercond. Nov. Magn. **27**, 1553–1560 (2014). https://doi.org/10.1007/s10948-013-2474-z
8. Li, L., Liang, L., Wu, H., Zhu, X.: One-dimensional perovskite manganite oxide nanostructures: recent developments in synthesis, characterization, transport properties, and applications. Nanoscale Res. Lett. **11**, 121 (2016). https://doi.org/10.1186/s11671-016-1320-1
9. Yi, C., Lin, B., Sun, Y., Yang, H., Zhang, X.: Structure, morphology and electrochemical properties of $La_xSr_{1-x}Co_{0.1}Mn_{0.9}O_{3-\delta}$ perovskite nanofibers prepared by electrospinning method. J. Alloys Compd. **624**, 31–39 (2015). https://doi.org/10.1016/j.jallcom.2014.10.178
10. Moghaddam, H.M., Nasirian, S.: Dependence of activation energy and lattice strain on TiO2 nanoparticles? Nanoscience Methods. **1**(1), 201–212 (2012). https://doi.org/10.1080/17458080.2011.620023
11. Shang, C., Guo, S., Wang, R.: Positive to negative ZFC exchange bias in $La_{0.5}Sr_{0.5}Mn_{0.8}Co_{0.2}O_3$ ceramics. Sci. Rep. **6**(25703), (2016). https://doi.org/10.1038/srep25703
12. Selmi, R., Cherif, W., Barquín, L.F., de la Fuente Rodríguez, M., Ktari, L.: Structure and spin glass behavior in $La_{0.77}Mg_{0.23-x}MnO_3$ ($0 \le x \le 0.2$) manganites. J. Alloys Compd. **738**, 528–539 (2018). https://doi.org/10.1016/j.jallcom.2017.12.189
13. Ling, L., Zhang, L., Zhang, Z., Pi, L., Tan, S., Zhang, Y.: Cluster-glass state and the effect of A-site magnetism in electron-doped

manganites. Solid State Commun. **149**, 1168–1172 (2009). https://doi.org/10.1016/j.ssc.2009.05.005
14. Fertman, E., Dolya, S., Desnenko, V., Beznosov, A., Kajnaková, M., Feher, A.: Cluster glass magnetism in the phase separated Nd2/3Ca1/3MnO3 perovskite. J. Magn. Magn. Mater. **324**, 3213–3217 (2012). https://doi.org/10.1016/j.jmmm.2012.05.043
15. Tiwari, P., Rath, C.: Evolution of structure and magnetic properties of stoichiometry and oxygen rich $LaMnO_3$ nanoparticles. J. Magn. Magn. Mater. **441**, 635–641 (2017). https://doi.org/10.1016/j.jmmm.2017.06.020
16. Ade, R., Singh, R.: Effect of grain size on charge and spin correlations in $Bi_{0.5}Ca_{0.5}MnO_3$ manganite nanoparticles. J. Magn. Magn. Mater. **418**, 273–279 (2016). https://doi.org/10.1016/j.jmmm.2016.02.028
17. Rostamnejadi, A., Venkatesan, M., Salamati, H., Ackland, K., Gholizadeh, H., Kameli, P., Coey, J.M.D.: Magnetic properties, exchange bias, and memory effects in core-shell superparamagnetic nanoparticles of $La_{0.67}Sr_{0.33}MnO_3$. J. Appl. Phys. **121**, 173902 (2017). https://doi.org/10.1063/1.4982893
18. Joy, P.A., Kumar, P.S.A., Date, S.K.: The relationship between field-cooled and zero-field-cooled susceptibilities of some ordered magnetic systems. J. Phys. Condens. Matter. **10**, 11049 (1998). http://iopscience.iop.org/0953-8984/10/48/024)
19. Issaoui, F., Bejar, M., Dhahri, E., Bekri, M., Lachkar, P., Hlil, E.K.: Crystal, spin glass, Griffiths phases and magnetocaloric properties of the $Sr_{1.5}Nd_{0.5}MnO_4$ compound. Physica B. **414**, 42–49 (2013). https://doi.org/10.1016/j.physb.2012.12.039
20. Zhang, Y.: Magnetic relaxation behavior in Tb-doped perovskite manganite. J. Magn. Magn. Mater. **323**, 1–3 (2011). https://doi.org/10.1016/j.jmmm.2010.08.045
21. Pana, O., Soran, M.L., Leostean, C., Macavei, S., Gautron, E., Teodorescu, C.M., Gheorghe, N., Chauvet, O.: Interface charge transfer in polypyrrole coated perovskite manganite magnetic nanoparticles. J. Appl. Phys. **111**, 044309 (2012). https://doi.org/10.1063/1.3686662?ver=pdfcov
22. Nisha, P., Pillai, S.S., Varma, M.R., Suresh, K.G.: Influence of cobalt on the structural, magnetic and magnetocaloric properties of $La_{0.67}Ca_{0.33}MnO_3$. J. Magn. Magn. Mater. **327**, 189–195 (2013). https://doi.org/10.1016/j.jmmm.2012.09.029
23. Manh, D.H., Phong, P.T., Nam, P.H., Tung, D.K., Phuc, N.X., Lee, I.-J.: Structural and magnetic study of $La_{0.7}Sr_{0.3}MnO_3$ nanoparticles and AC magnetic heating characteristics for hyperthermia applications. Physica B. **444**, 94–102 (2014)
24. Londoñoo-Calderon, V., Rave-Osorio, L.C., Restrepo, J., Játiva, J., Jurado, J.F., Arnache, O., Restrepo-Parra, E.: Structural and magnetic properties of La_{1-x} $(Ca,Sr)_xMnO_3$ powders produced by the hydrothermal method. J. Supercond. Nov. Magn. **31**, 4153–4162 (2018). https://doi.org/10.1007/s10948-018-4625-8
25. C. A. Cardoso, F. M. Araujo-Moreira, V. P. S. Awana, E. Takayama-Muromachi, O. F. de Lima, H. Yamauchi and M. Karppinen. Spin glass behavior in $RuSr_2Gd_{1.5}Ce_{0.5}Cu_2O_{10-\delta}$, Phys. Rev. B 67, 020407(R) (2003). DOI: https://doi.org/10.1103/PhysRevB.67.020407
26. Patricia Darlene Mitchler. Characterization of Hysteresis in Magnetic Systems: A Preisach Approach (PhD Thesis) (2000). Department of Physics and Astronomy, University of Manitoba, Winnipeg, Manitoba
27. Kumar, A., Tandon, R.P., Awana, V.P.S.: Successive spin glass, cluster ferromagnetic and superparamagnetic transitions in $RuSr_2Y_{1.5}Ce_{0.5}Cu_2O_{10}$ complex magneto-superconductor. Eur. Phys. J. B. **85**(238), (2012). https://doi.org/10.1140/epjb/e2012-30075-5